DOI: 10.1002/ange.201310714

Photo-annealing

# A Photo-annealing Approach for Building Functional Polymer Layers on Paper**

*Qiuping Qian, Jian Wang, Feng Yan, and Yapei Wang**

***Abstract:*** *A straightforward photo-annealing approach was developed for building functional polymer layers on paper. Conducting polyaniline with the ability for photothermal conversion can be readily annealed by near-infrared light. The annealed polymers become both insulating and hydrophobic. Selective photo-annealing produces a functional layer with patterned conductive arrays. This material exhibits real-time response to ammonium gas. Complete photo-annealing preserves the porous structure but changes the wettability of the polyaniline-nanofiber film.*

Annealing treatments are commonly used to refine the nano- or micro-structures of polymeric materials by inducing changes in physical properties and phase separation. General annealing strategies, including thermal annealing and solvent annealing, are used to soften and reorganize polymer chains.[1] Regardless of scalability and simplicity, both methods are incapable of partial or selective annealing. The whole polymer film together with the supporting substrates has to be subjected to high temperatures or solvent vapors.[2] Inevitable destruction of the fragile substrates and poor control of the annealing area become important and pervasive problems. Photo-annealing by using intense light sources, for example, powerful lasers, can generate localized heat, thereby affording the convenience of melting polymers within a specific region.[3] However, the deep penetration of incident light can also cause thermal damage to the underlying substrate, thus limiting the use of photo- or thermo-labile supporting materials.

Rarely has attention been paid to achieving photo-annealing through the use of near-infrared (NIR) light with low irradiation doses. Mild NIR light can illuminate a desired position and causes little damage to supporting materials, however, the energy may be insufficient to soften the polymers. Dark materials with the ability to undergo photo-thermal conversion can satisfy this demand. Our previous work revealed that carbon nanotubes can tailor a rapid phase transition of individual polymer particles by NIR light.[4] Conducting polymers with deep color, in addition to distinct electrical performance, are able to absorb light with a wide range of wavelengths and generate heat without the aid of other agents.[5] Such photothermal conversions have been investigated as powerful tools for killing cancer cells in biological systems[6] or welding polymers in the dry state.[7]

A popular supporting material for preparing portable devices is cellulose paper owing to its high flexibility and low cost. Photo-annealing of conducting polymers paves the way to building functional layers on this fragile substrate. In this work, a rapid photo-annealing of polyaniline nanofibers on cellulose paper was remotely accomplished through the use of NIR light. Along with a change in their nanostructures, the conducting polymers undergo changes to their electrical performance and wettablity. Besides its simplicity and generality, photo-annealing has two particular merits for modifying polyaniline on paper: 1) it affords great convenience for selective annealing to fabricate conducting arrays with desired pattern features, and 2) it is not damaging to the supporting materials if low-power light is used, thus leading to the formation of an asymmetric filter membrane.

A general route for building functional layers on cellulose paper is illustrated in Figure 1. A cellulose filter paper coated with a layer of polyaniline nanofibers (Figure 1 b) was exposed to mild NIR light. The polyaniline nanofibers rapidly melted, concomitantly forming agglomerates within the exposed area. Such photo-annealed areas can be clearly distinguished from surroundings because of their altered color (Figure 1 c). To prepare water-dispersible polyaniline nanofibers, a versatile interfacial polymerization was accomplished between a dichloromethane phase consisting of aniline and a water phase containing dissolved $FeCl_3$.[8] Polyaniline nanofibers were quickly formed at the interface owing to the oxidation of aniline by $FeCl_3$. As shown in Figure 2, this interfacial polymerization offers extraordinary control of the nanostructure of the polyaniline nanofibers. The nanofibers became thicker and branched upon increasing the oxidant concentration. Thinner nanofibers (Figure 2 b) were hardly retained on the paper during a suction filtration process. However, the unique branched morphology (Figure 2 h) acquired at high concentrations of $FeCl_3$ prevented the nanofibers from penetrating the paper, thus enabling optimal deposition of a polyaniline-nanofiber film onto paper. It should be noted that the use of saturated $FeCl_3$ also improved the polymerization capacity, thus leading to the generation of more nanofibers. As shown in Figure 2 i, a standard batch of polymerization formulation, including

[*] Q. Qian, J. Wang, Prof. Y. Wang
Department of Chemistry, Renmin University of China
Beijing, 100872 (China)
E-mail: yapeiwang@ruc.edu.cn
Prof. F. Yan
School of Chemistry and Chemical Engineering
Soochow University at Dushuhu Lake, Suzhou, 215123 (China)

[**] This work was financially supported by the National Natural Science Foundation of China (51373197), Trans-Century Training Programme Foundation for the Talents by the State Education Commission (NCET-12-0530), and Jiangsu Key Laboratory of Advanced Functional Polymer Design and Application (Soochow University).

Supporting information for this article is available on the WWW under http://dx.doi.org/10.1002/anie.201310714.

 © 2014 Wiley-VCH Verlag GmbH & Co. KGaA, Weinheim 

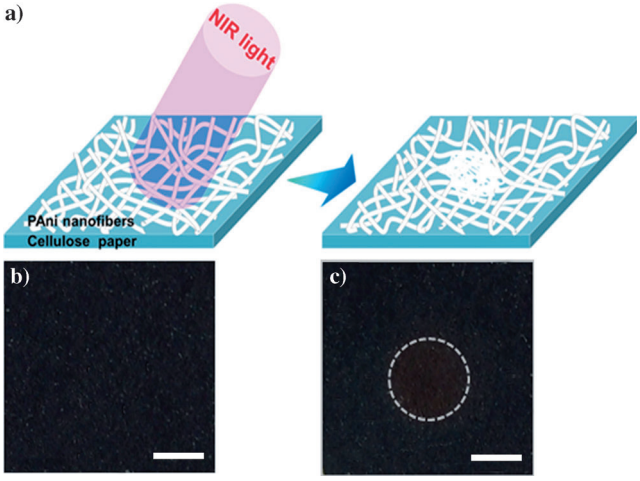


***Figure 1.*** a) Schematic illustration of photo-annealing of polyaniline nanofibers on cellulose paper. Photographic images of polyaniline nanofibers film on a filter paper before (b) and after (c) NIR light treatment (2 $Wcm^{-2}$). The annealed area is marked with a dashed circle. Scale bar: 5 mm.

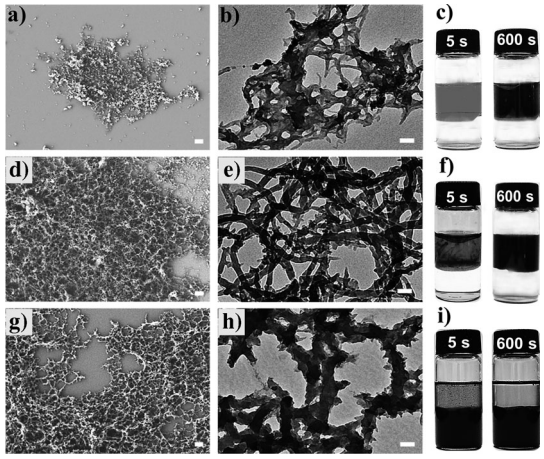


***Figure 2.*** SEM (a, d, g) and TEM (b, e, h) images of polyaniline nanofibers to show the morphological evolution of the polyaniline nanofibers when using the oxidant $FeCl_3$ at different concentrations: 0.25 M (a, b), 1.0 M (d, e), 5.67 M (g, h). Photographic images of the formation of polyaniline after contract between the aniline phase and the $FeCl_3$ phase taken after 5 s and 10 min. The concentrations of $FeCl_3$ is 0.25 M (c), 1.0 M (f) and 5.67 M (i). The aniline concentration is 1.0 M. The scale bars of the SEM and TEM images are 1 μm and 50 nm, respectively.

aniline (1.0 M, 4 mL) and $FeCl_3$ (5.67 M, 4 mL), can ultimately produce 25 mg polyaniline nanofibers in 10 min.

Photoirradiation under NIR light is able to actuate an electrical response in polyaniline nanofibers on the basis of the change in their conductivity. In order to validate this assertion, an electrical device was fabricated by bridging a paper chip deposited with a layer of polyaniline nanofibers (15 μm in thickness) with two gold electrodes (Figure S1 in the Supporting Information). This paper device outputs electrical signals on an electrochemical workstation with an applied direct voltage. To quantitatively view the photoresponse, the signal output was normalized by the absolute change of conductivity ($-\Delta G/G_0$) as in the following equation:

$$-\Delta G/G_0\,\% = [(I_0 - I)/I_0]\,100\,\%$$

where $G_0$ and $I_0$ are the initial conductivity and current before the photoirradiation, and $I$ is the current after exposure to NIR light with a specific power density. To our surprise, the conductivity increased abruptly at the beginning of photoirradiation, whereas it dropped quickly with extension of the light irradiation (Figure 3a). The initial increase in conductivity is hypothesized to be due to the photo-effect of the NIR light (Figure S2). It is assumed that the excitons generated by light illumination dissociated into free electrons and holes, thus instantly improving the conductivity of polyaniline nanofibers.[9] This hypothesis is verified by a camera flashing with short exposure time. As shown in Figure 3b, a sharp increase in conductivity occurs at each exposure. With prolonged NIR irradiation, the thermo-effect becomes dominant. Photothermal conversion by polyaniline nanofibers generates a lot of heat, thereby significantly raising the local temperature within the conducting fibers. Rather than improving the conductivity as increased temperature usually does in semiconductors, the rising temperature caused by light irradiation enables the annealing of the proton-doped poly-

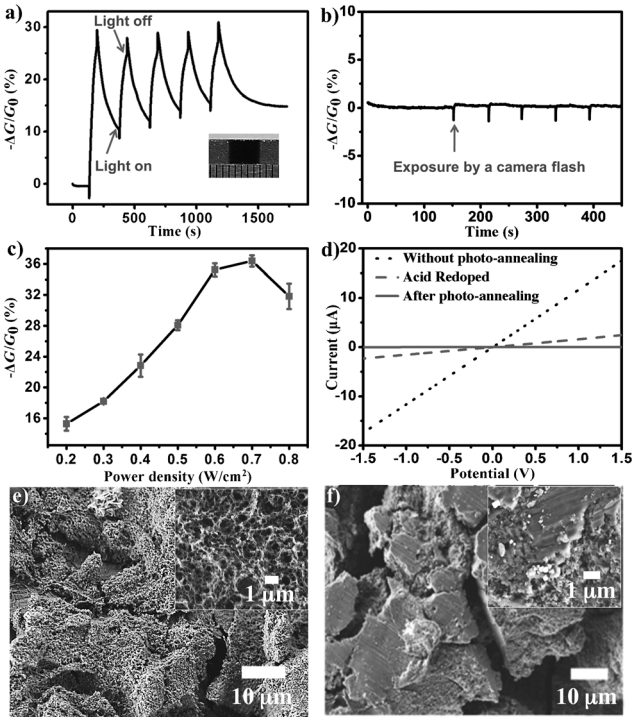


***Figure 3.*** a) On–off cycles of the NIR response of a paper device. The NIR light intensity is 0.2 $Wcm^{-2}$. Inset: a typical paper chip 5 mm × 5 mm square. b) Cycles of the conductivity change caused by a camera flashing. c) The normalized conductivity change relating to light intensities ranging from 0.2—0.8 $Wcm^{-2}$. d) Typical *I–V* curves acquired with a paper device consisting of a layer of polyaniline nanofibers before NIR light treatment, after NIR light treatment (2 $Wcm^{-2}$), and after acid redoping. SEM images of a film composed of polyaninline nanofibers on a filter paper before (e) and after (f) NIR light treatment (2 $Wcm^{-2}$) are shown.


© 2014 Wiley-VCH Verlag GmbH & Co. KGaA, Weinheim

aniline nanofibers, thereby causing an irreversible reduction in the conductivity. A critical temperature was determined as 90 °C on a heating plate: temperatures higher than this value have a negative effect on the conductivity (Figure S3). This critical temperature should have been exceeded by the temperature rise associated with the photothermal conversion. The conductivity change becomes greater upon increasing the dose of NIR irradiation, yet it falls when the power density is over 0.7 $W cm^{-2}$ (Figure 3c). It should be noted that the paper device becomes completely insulating if it is annealed by light with a power density of 2 $W cm^{-2}$ for 1.5 min.

The irreversible decrease in conductivity induced by photo-annealing is attributed to phase transition and dedoping. As shown in Figure 3e and f, the interpenetrating network of nanofibers on a paper substrate was turned into an irregular polymer film after severe irradiation for one minute. As stated above, the photothermal conversion is efficient because most of the light energy is confined within the network. The rising temperature is thought to be high enough to melt the nanofibers. At the state of phase transition, crosslinking and chain oxidation may occur. Both of these processes impair the conductivity of polyaniline. Analysis of the Fourier transformed infrared (FT-IR) spectrum revealed dramatic changes in the relative intensities of the peaks centered at 1497, 1297 and 820 $cm^{-1}$, thus indicating crosslinking of the polyaniline.[10] A weak peak at 1758 $cm^{-1}$ suggests a partial oxidation of the polyaninline (see Figure S5). High local temperature may cause the loss of dopants from the polyaniline. The conductance is fully recovered if the paper device annealed by low intensity light is redoped by hydrochloric acid (Figure S4), thus indicating that dedoping also contributes to impairing the conductance. However, the conductance is only partially recovered by redoping if the paper device is annealed by high intensity light, as shown in Figure 3d. It can be concluded that dedoping causes a recoverable conductance decrease in the polyaniline while the occurrence of chemical reactions on strong light treatment results in permanent destruction of the conjugative structure.

The transition from a conductive to an insulating state affords great promise for constructing functional layers on paper with patterned conductance. Selective photo-annealing was achieved through the use of a striped mask on a paper chip, as illustrated in Figure 4a. The exposed area becomes electrically insulated, while the covered area retains conductive performance. The paper chip has a low surface resistance of several KΩ in the longitudinal direction but the lateral resistance is infinite (Figure 4b). Owing to the sensitive of polyaniline to Lewis base, a thorough sensing assessment of the paper chips with conductive arrays was conducted by using ammonia. It has been widely accepted that ammonia can neutralize the doped protons of polyaniline, thereby leading to conversion of the conductive emeraldine salt to the insulating emeraldine base (Figure 4c).[11] Sensing devices with control over array length and width were electrically bridged by two gold electrodes. As shown in Figure 4d, the conductivity change ($-\Delta G/G_0$) grows to a plateau within few seconds when the device is placed in a thin ammonia atmosphere with a concentration of 50 ppm.

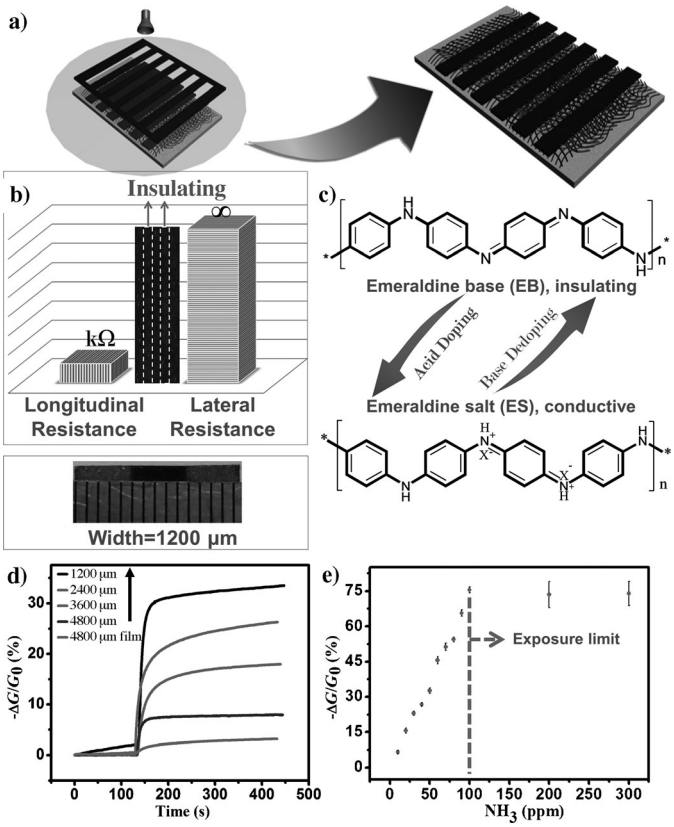


***Figure 4.*** a) Schematic illustration of selective photo-annealing through a striped mask. b) The longitudinal and lateral resistance of a paper chip after selective photo-annealing by NIR light (2 $W cm^{-2}$). c) Chemical structures of the insulating emeraldine base and conductive emeraldine salt. d) The $NH_3$ response of paper chips with four polyaniline nanofiber arrays of line width 1200 μm, 2400 μm, 3600 μm, and 4800 μm. A control polyaniline film with width of 4800 μm was produced by vapor polymerization. The $NH_3$ concentration is 50 ppm. e) Sensing test of paper chips with one line of 1200 μm array in the presence of $NH_3$ with concentrations ranging from 10 ppm to 300 ppm. The gap between two electrodes is 0.5 cm.

Narrowing the array width can dramatically improve the sensitivity of detection.[12] The conductivity change of a $\times$1200 μm array is five times larger than that of a $\times$4800 μm array. Furthermore, because the network of nanofibers provides a larger surface area, the polyaniline-nanofiber-based paper device is superior to a paper device with a polyaniline film produced through vapor phase polymerization and exhibits better performance in recognizing ammonium gas. The theoretical detection limit (DL) was estimated by analyzing a sensing curve at 50 ppm ammonia, with 100 consecutive points randomly selected to calculate the standard deviation (Figure 4e). DL varies with the standard deviation (SD) of blank values and the average peak height (APH) according to the relationship $DL = 3SD \times 50/APH$. A detection limit of 0.25 ppm was obtained from the calculation result. Excessive exposure did not cause the sensing chip to output stronger signals when the ammonia concentration was over 100 ppm (Figure 3c). However, this exposure limit is already three times higher than the point at which ammonia can be detected by the human nose.


© 2014 Wiley-VCH Verlag GmbH & Co. KGaA, Weinheim

In addition to the change in electrical performance, the surface wettability of polyaniline nanofibers can be changed by photo-annealing. As shown in Figure 5a, the film consisting of polyaniline nanofibers on filter paper was hydrophilic and water was quickly absorbed. However, the film became hydrophobic with a contact angle of 132° owing to the loss of dopants after an adequate photo-annealing (Figure 5b).

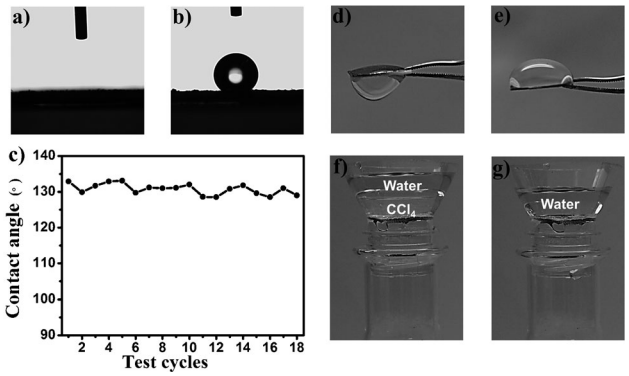


***Figure 5.*** Photographs of water droplets on the polyaniline nanofiber film before (a) and after (b) photo-annealing. c) Repeated contact angle measurements at fixed position after each water droplet was completely adsorbed into the film. Photographic image are shown of water injected onto the polyaniline surface (d) and the paper surface (e). Water/carbon tetrachloride separation by the asymmetric film is shown at the beginning (f) and after completion (g).

Interestingly, the water droplet gradually entered the hydrophobic film after standing on the surface for a few seconds (Video S1, S2). The contact angle of the region where water entered remained high, thus indicating that surface wettability was not influenced by water (Figure 5c). The rear layer of filter paper was found to be wetted by water droplets. Notably, one-way penetration is directed by the asymmetric structure with the combination of a hydrophobic film and a hydrophilic rear layer. Water injected onto the polyaniline surface passed through the structure as it was absorbed by the rear paper layer (Figure 5d). Turning the film over, water did not penetrate through the paper (Figure 5e). Mercury porosimetry revealed that the annealed polyaniline film retained porous features although the pore size distribution was shifted downwards (Figure S6). Water overcomes the porous barrier owing to powerful attraction by the backing paper. Through acting as a "water-diode", the asymmetric paper is envisioned to harvest and pump water in a controlled manner. Additionally, the functional paper was readily extended to water/oil separation, and only allowed apolar solvent to pass through (Figure 5f,g).

In summary, we have demonstrated a straightforward and generally applicable photo-annealing approach for building functional polymer layers on paper. Conducting polyaniline with the ability to undergo photothermal conversion can be readily annealed by near-infrared light. The annealed area changes to become insulating and hydrophobic. Selective photo-annealing produces a functional layer with patterned conductive arrays. This material exhibits real-time response to ammonium gas. Complete photo-annealing preserves the porous features but changes the wettability of the polyaniline film. The asymmetric paper functions as a "water diode", thus allowing water to pass only from the annealed layer towards the backing paper. This paper material is intriguing. In addition to facilitating oil/water separation, it could potentially extended to clinical applications, for example, vacuum assisted closure to treat wounds. Other light-absorbing materials, including some conventional polymers and supramolecular blends, will be considered for exploiting new functions through photo-annealing.

Received: December 10, 2013
Revised: January 15, 2014
Published online: March 13, 2014

**Keywords:** conducting materials · gas sensors · paper devices · polymers · photo-annealing

[1] a) L. Xue, Y. Han, *Prog. Polym. Sci.* **2011**, *36*, 269–293; b) H. Chen, S. Hu, H. Zang, B. Hu, M. Dadmun, *Adv. Funct. Mater.* **2013**, *23*, 1701–1710; c) J. Vogelsang, J. Brazard, T. Adachi, J. C. Bolinger, P. F. Barbara, *Angew. Chem.* **2011**, *123*, 2305–2309; *Angew. Chem. Int. Ed.* **2011**, *50*, 2257–2261; d) H. Yao, G. Huang, C. Cui, X. Wang, S. Yu, *Adv. Mater.* **2011**, *23*, 3643–3647.

[2] a) K. Y. Law, *Chem. Rev.* **1993**, *93*, 449–486; b) S. Miller, G. Fanchini, Y. Y. Lin, C. Li, C. W. Chen, W. F. Su, M. Chhowalla, *J. Mater. Chem.* **2008**, *18*, 306–312; c) T. M. Clarke, A. M. Ballantyne, J. Nelson, D. D. C. Bradley, J. R. Durran, *Adv. Funct. Mater.* **2008**, *18*, 4029–4035; d) S. Park, B. Kim, J. Xu, T. Hofmann, B. Ocko, T. Russell, *Macromolecules* **2009**, *42*, 1278–1284.

[3] a) K. Kim, J. Y. Woo, S. Jeong, C.-S. Han, *Adv. Mater.* **2011**, *23*, 911–914; b) M. Lilliedal, A. Medford, M. Madsen, K. Norrman, F. Krebs, *Sol. Energy Mater. Sol. Cells* **2010**, *94*, 2018–2031.

[4] a) X. Huang, Q. Qian, X. Zhang, W. Du, H. Xu, Y. Wang, *Part. Part. Syst. Charact.* **2013**, *30*, 235–240; b) Q. Qian, X. Huang, X. Zhang, Z. Xie, Y. Wang, *Angew. Chem.* **2013**, *125*, 10819–10823; *Angew. Chem. Int. Ed.* **2013**, *52*, 10625–10629.

[5] H. Jia, J. Wang, X. Zhang, Y. Wang, *ACS Macro Lett.* **2014**, *3*, 86–90.

[6] K. Yang, H. Xu, L. Cheng, C. Sun, J. Wang, Z, Liu, *Adv. Mater.* **2012**, *24*, 5586–5592.

[7] a) J. Huang, R. Kaner, *Nat. Mater.* **2004**, *3*, 783–786; b) D. Li, J. Huang, R. B. Kaner, *Acc. Chem. Res.* **2009**, *42*, 135–145.

[8] J. Huang, R. B. Kaner, *J. Am. Chem. Soc.* **2004**, *126*, 811–855.

[9] B. Pradhan, K. Setyowati, H. Liu, D. H. Waldeck, J. Chen, *Nano Lett.* **2008**, *8*, 1142–1146.

[10] a) S. S. Pandey, M. Gerard, A. L. Sharma, B. D. Malhotra, *J. Appl. Polym. Sci.* **2000**, *75*, 149–155; b) R. Mathew, B. R. Mattes, M. P. Espe, *Synth. Met.* **2002**, *131*, 141–147.

[11] a) D. Nicolas-Debarnot, F. Poncin-Epaillard, *Anal. Chim. Acta* **2003**, *475*, 1–15; b) M. Ding, Y. Tang, P. Gou, M. Reber, A. Star, *Adv. Mater.* **2011**, *23*, 536–540.

[12] J. Wang, X. Zhang, X. Huang, S. Wang, Q. Qian, W. Du, Y. Wang, *Small* **2013**, *9*, 3759–3764.

 © 2014 Wiley-VCH Verlag GmbH & Co. KGaA, Weinheim 